

# Carbonate Assimilation at Merapi Volcano, Java, Indonesia: Insights from Crystal Isotope Stratigraphy

JANE P. CHADWICK<sup>1\*</sup>, VALENTIN R. TROLL<sup>1</sup>, CATHERINE GINIBRE<sup>2,3</sup>, DANIEL MORGAN<sup>2,4</sup>, RALF GERTISSER<sup>5</sup>, TOD E. WAIGHT<sup>6</sup> AND JON P. DAVIDSON<sup>2</sup>

<sup>1</sup>DEPARTMENT OF GEOLOGY, THE UNIVERSITY OF DUBLIN, TRINITY COLLEGE, DUBLIN 2, IRELAND

<sup>2</sup>DEPARTMENT OF EARTH SCIENCES, UNIVERSITY OF DURHAM, SOUTH ROAD, DURHAM DH1 3LE, UK

<sup>3</sup>DEPARTMENT OF MINERALOGY, UNIVERSITY OF GENEVA, RUE DES MARAÎCHERS, 13 CH-1205, GENEVA, SWITZERLAND

<sup>4</sup>SCHOOL OF EARTH AND ENVIRONMENT, UNIVERSITY OF LEEDS, LEEDS LS2 9JT, UK

<sup>5</sup>SCHOOL OF PHYSICAL AND GEOGRAPHICAL SCIENCES, KEELE UNIVERSITY, KEELE ST5 5BG, UK

<sup>6</sup>GEOLOGICAL INSTITUTE, ØSTER VOLDGADE 10, 1350 COPENHAGEN K, DENMARK

RECEIVED JANUARY 29, 2007; ACCEPTED JULY 3, 2007  
ADVANCE ACCESS PUBLICATION AUGUST 16, 2007

Recent basaltic andesite lavas from Merapi volcano contain abundant, complexly zoned, plagioclase phenocrysts, analysed here for their petrographic textures, major element composition and Sr isotope composition. Anorthite (*An*) content in individual crystals can vary by as much as 55 mol% ( $An_{40-95}$ ) across internal resorption surfaces with a negative correlation between high *An* mol% (>70), MgO wt% and FeO wt%. In situ Sr isotope analyses of zoned plagioclase phenocrysts show that the  $^{87}\text{Sr}/^{86}\text{Sr}$  ratios of individual zones range from 0.70568 to 0.70627. The upper end of this range is notably more radiogenic than the host basaltic andesite whole-rocks (<0.70574). Crystal zones with the highest *An* content have the highest  $^{87}\text{Sr}/^{86}\text{Sr}$  values, requiring a source or melt with elevated radiogenic Sr, rich in Ca and with lower Mg and Fe. Recent Merapi eruptive rocks contain abundant xenoliths, including metamorphosed volcanoclastic sediment and carbonate country rock (calc-silicate skarns) analysed here for petrographic textures, mineralogy, major element composition and Sr isotope composition. The xenoliths contain extremely calcic plagioclase (up to  $An_{100}$ ) and have whole-rock  $^{87}\text{Sr}/^{86}\text{Sr}$  ratios of 0.70584 to 0.70786. The presence of these xenoliths and their mineralogy and geochemistry, coupled with the  $^{87}\text{Sr}/^{86}\text{Sr}$  ratios observed in different zones of individual phenocrysts, indicate that magma–crust interaction at Merapi is

potentially more significant than previously thought, as numerous crystal cores in the phenocrysts appear to be inherited from a metamorphosed sedimentary crustal source. This has potentially significant consequences for geochemical mass-balance calculations, volatile saturation and flux and eruptive behaviour at Merapi and similar island arc volcanic systems elsewhere.

KEY WORDS: assimilation; isotopes; Merapi; xenolith; calc-silicate

## INTRODUCTION

Merapi volcano, in Central Java, Indonesia, is currently one of the most active volcanoes on Earth, with eruptions having occurred in historical and prehistoric times (Voight *et al.*, 2000). Arc magmas, such as those erupted at Merapi volcano, typically display chemical and petrographic characteristics indicative of crustal contamination (Hildreth & Moorbath, 1988; Davidson *et al.*, 1990). However, identification of a crustal component in magma genesis often yields limited information about where and when this contamination has taken place; at source, or in the crust during

\*Corresponding author. Telephone: +35318962675.  
E-mail: chadwj@td.ie

subsequent ascent. Contamination of Merapi and Sunda arc magmas by calcareous sediments was considered by previous workers (Hemond, 1986; Luais, 1986; Turner & Foden, 2001); however, isotopic heterogeneity in recent Merapi basaltic andesites has been largely attributed to source contamination deep in the Sunda arc subduction zone system, based on whole-rock geochemical data (Gertisser & Keller, 2003a; Debaille *et al.*, 2006). Those workers argued that shallow contamination at Merapi played an insignificant role because of a lack of systematic variation in whole-rock isotope compositions with SiO<sub>2</sub>. Trends towards elevated whole-rock δ<sup>18</sup>O values were attributed to possible post-eruptive hydration and exchange of oxygen between ground water and volcanic glass (Gertisser & Keller, 2003a).

Increasing numbers of *in situ* isotope studies, however, have highlighted the limitations inherent in whole-rock isotope analysis of phenocryst-rich volcanic rocks (e.g. Davidson & Tepley, 1997; Wolff *et al.*, 1999; Ramos *et al.*, 2005). These studies have identified heterogeneity at the mineral and sub-mineral scale, with whole-rock isotopic ratios regarded as representing the sum of the magma's component parts. *In situ* isotope profiles measured across a phenocryst may record petrogenetic processes that are

masked in the whole-rock isotope ratios. In addition, the technique has been utilized to identify the presence of xenocrysts in various magmatic systems (e.g. Perini *et al.*, 2003).

Using crystal isotope stratigraphy (Davidson & Tepley, 1997), and by analysing xenoliths hosted in recent deposits, we have identified the operation of complex, shallow-level, open-system processes at Merapi volcano. We argue that although source contamination may play an important role in Merapi magma petrogenesis, the occurrence of shallower processes is significant and has important repercussions for magma evolution, mass-balance modelling, the CO<sub>2</sub> budget and potentially eruptive behaviour for this high-risk volcano.

## GEOLOGICAL BACKGROUND

Merapi volcano is a large Quaternary stratovolcano situated on the active volcanic front of the Sunda arc in Central Java (Fig. 1). This volcanism is the result of the northward subduction of the Indo-Australian plate beneath the Eurasian plate (Hamilton, 1979; Jarrard, 1986) at a rate of  $\sim 6.7 \pm 0.7$  cm/year (Tregoning *et al.*, 1994). The active arc in Central and East Java is bounded to the south by the

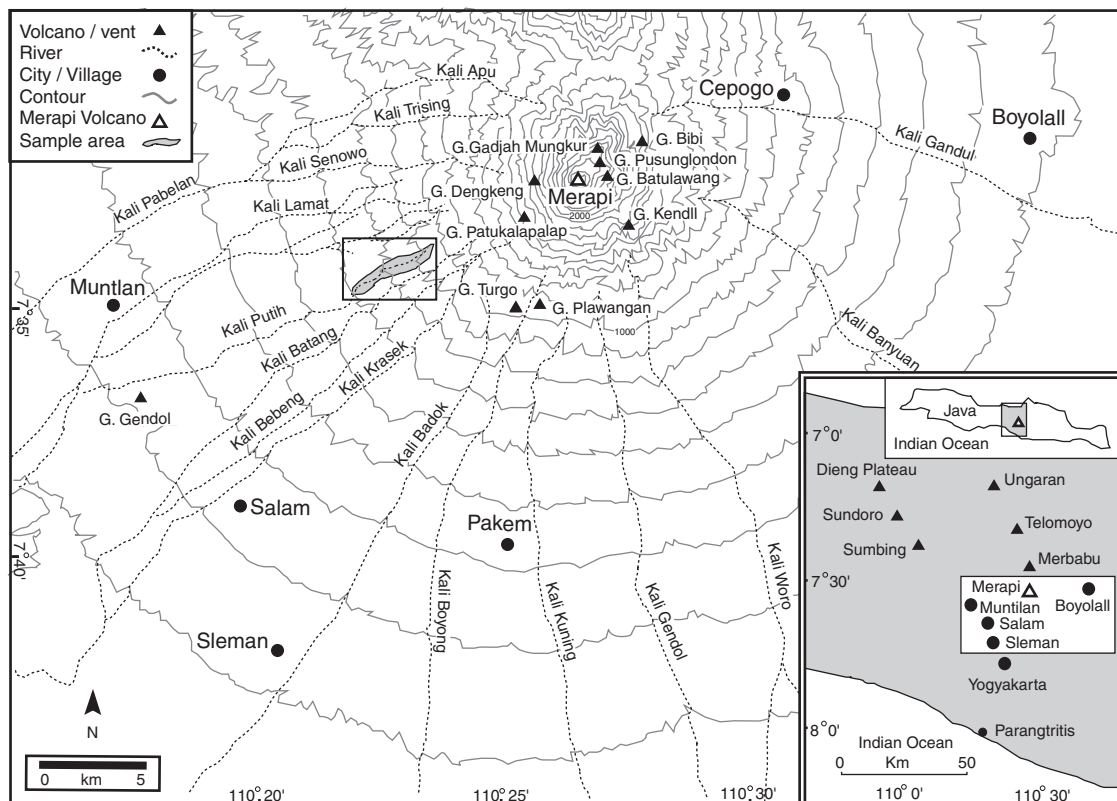


**Fig. 1.** Sketch map of the summit of Merapi with inset showing the location of Merapi relative to other Quaternary volcanoes in the area (triangles) and areas of significant population (●) in Central Java (from Gertisser & Keller, 2003b). Sampling location at Kali Putih highlighted in grey.

Southern Mountains Zone, eroded remnants of the Eocene to Miocene volcanic arc, and to the north by the Kendeng basin, the main Cenozoic depocentre for the region (Smyth *et al.*, 2005). The Kendeng basin is thought to contain between 8 km (de Genevraye & Samuel, 1972) and 11 km (Untung & Sato, 1978) of sediment. These volcanic and sedimentary lithologies overlie a basement of uncertain composition that has been referred to as quasi-continental, immature, arc-crust, which extends to depths of ~25 km below the surface (van Bemmelen, 1949; Curray *et al.*, 1977; Jarrard, 1986). The upper crust exposed in the area is composed of a sequence of Cretaceous to Tertiary marine limestones, marls and volcanoclastic sediment with units up to 2 km thick (van Bemmelen, 1949) that crop out proximal to Merapi and can be found as abundant, thermally metamorphosed xenoliths (Fig. 2) in recent lavas (see Camus *et al.*, 2000). Exposure is rare because of dense tropical vegetation and habitation in the area surrounding the volcano and there is limited further information on the nature of the crust in this area in the recent literature.

Ratdomopurbo & Poupinet (2000) reported the presence of an aseismic zone at a depth of ~2.5–3 km below the summit that was thought to indicate the existence of a possibly ephemeral, shallow melt pocket beneath Merapi. However, global positioning system (GPS) and tilt data (Beauducel & Cornet, 1999) discount the possibility of a magma reservoir in the Merapi edifice, as does published deformation data (Westerhaus *et al.*, 1998). In agreement with petrological data (Gertisser & Keller, 2003*b*), it is now thought that Merapi magmas are sourced from a deeper reservoir >5 km below sea level, with deeper magma storage chambers postulated on the basis of geobarometry studies and potential minor shallow-level storage, suggesting a quasi-steady-state magma supply system beneath the volcano (Gertisser, 2001; Chadwick *et al.*, in preparation).

Recent volcanic activity at Merapi has been largely restricted to extrusion of viscous lavas forming a dome complex in the summit area, with pyroclastic block-and-ash flows resulting from gravitational instability and

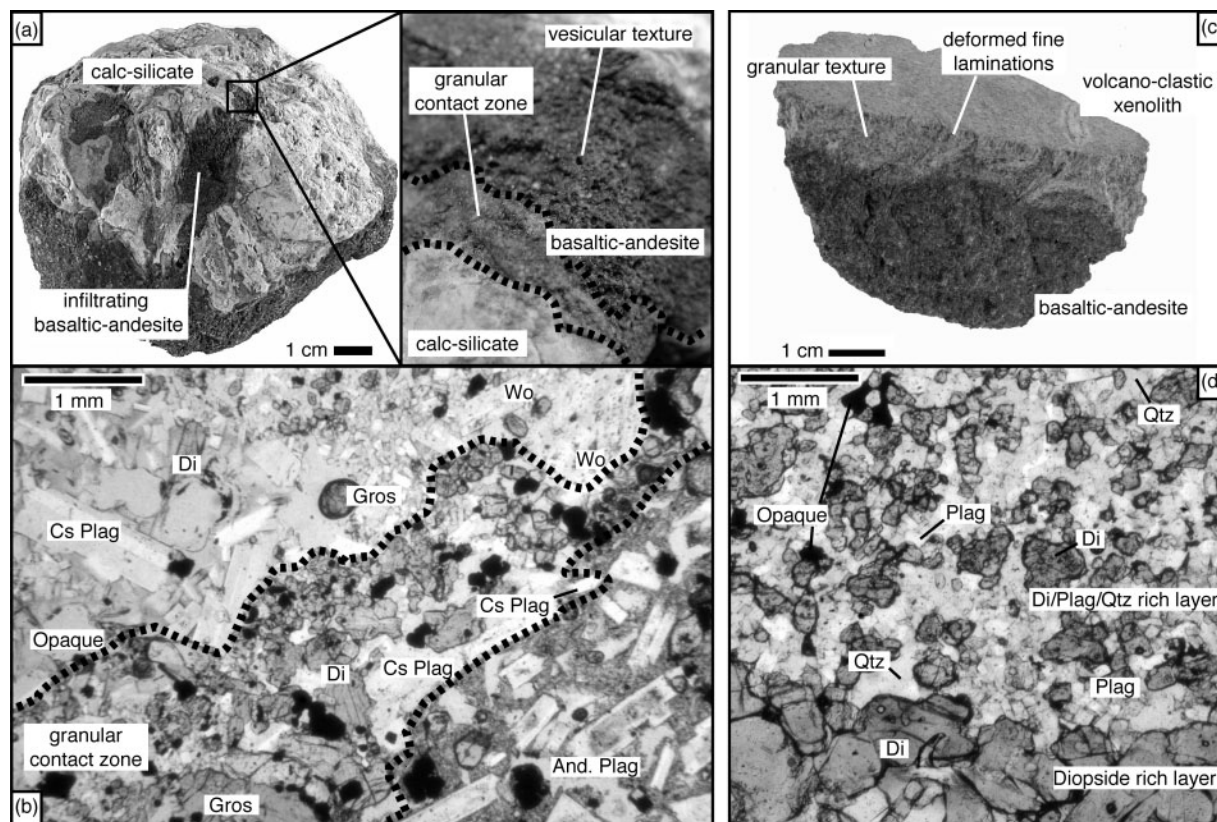


**Fig. 2.** (a) Representative calc-silicate xenolith (XCS-3), with well-developed reaction rim. Inset shows highly vesicular contact between calc-silicate and host andesite highlighted with dashed lines. (b) Photomicrograph (plane-polarized light; PPL) of calc-silicate xenolith–andesite contact zone highlighted with dashed lines. Contact zone is diffuse with plagioclase laths (Cs Plag), grossular (Gros), diopside (Di), and wollastonite (Wo) evident in the calc-silicate xenolith. Large zoned plagioclase (And. Plag) forms the dominant phase in the basaltic andesite. (c) Representative volcanoclastic xenolith (XCS-2), with sharp contact with host basaltic andesite and primary layering preserved. (d) Photomicrograph (PPL) of volcanoclastic xenolith illustrating variation in grain size and mineralogy between layers.

collapse of these domes (e.g. Voight *et al.*, 2000; Schwarzkopf *et al.*, 2001, 2005). Pyroclastic deposits are of basaltic andesite composition and are inclusion-rich. These inclusions may be classified into two groups (Troll *et al.*, 2003): igneous inclusions including enclaves and crystalline cumulates and variably metamorphosed xenoliths of sedimentary country rock (Fig. 2). The presence of these inclusions, particularly the metasedimentary xenoliths, suggests the operation of complex, shallow-level, magma chamber processes, particularly interaction between magma and local crust (see Renzulli *et al.*, 2001, 2003). Although their occurrence has been noted and samples have been described by previous workers (e.g. Clochiatti *et al.*, 1982; Kerinec, 1982; Camus *et al.*, 2000; Gertisser & Keller, 2003a), detailed geochemical analyses of these xenoliths and an investigation of their significance is presented here for the first time.

As is typical of many intermediate composition volcanic arcs, the recent eruptive products are generally highly porphyritic, containing up to 60% crystals by volume. Dominant mineral phases are plagioclase and clinopyroxene, with rare amphibole and titanomagnetite (Gertisser, 2001). The phenocrysts are set in a fine microcrystalline to glassy groundmass, and plagioclase and pyroxene crystals are typically complexly zoned. Geochemical variation within individual plagioclase crystals is considerable ( $An_{34-95}$ ).

A high-K, calc-alkaline suite of whole-rock compositions has been identified in recent Merapi volcanic rocks (<1900  $^{14}C$  years BP; Bahar, 1984; del Marmol, 1989; Hammer *et al.*, 2000; Gertisser & Keller, 2003a, 2003b). These samples display a relatively restricted spread in whole-rock isotope ratios, providing evidence for source contamination and minimal interaction with the upper crust (Gertisser & Keller, 2003a). However, Gasparon *et al.* (1994) reported considerable crustal contamination of recent Sunda arc lavas based on a He isotope study. The presence of numerous xenoliths in the recent Merapi deposits supports this finding and, combined with the complex zoning patterns observed in the dominant phenocryst phases, indicates that intra-crustal magmatic processes may be significant in Merapi's evolution. Given the high Sr content of the crystals (>600 ppm), complex zonation, and a crustal- to near-crustal stability field (see Ramos *et al.*, 2005), plagioclase is an ideal phase for identifying crustal petrogenetic processes at Merapi via *in situ* Sr isotope analysis.

## SAMPLING AND ANALYTICAL METHODS

### Samples

The samples for this study are basaltic andesite clasts and xenolith samples from the July 1998 block-and-ash flow deposits and local sedimentary country rock. Samples

from the 1998 block-and-ash flow were collected in September 2002, from Jurangero quarry at Kali (valley in Indonesian) Putih, just over 5 km SW of the Merapi summit (Fig. 1). These flow deposits are composed of three components: a basal avalanche, a low-density ground surge, and an ash layer (Schwarzkopf *et al.*, 2005). The basaltic andesite and xenolith samples analysed in this study are clasts from the poorly sorted basal avalanche, sourced from the 1998 dome. Decimetre- to centimetre-sized blocks are set in a fine ash matrix, with the largest blocks in the deposits typically between 1 and 3 m in size and rare exceptions of up to 20 m diameter. The clasts are dominantly juvenile material (up to 80% for clasts >3 cm) including highly porphyritic basaltic andesite and lesser scoria (between 5 and 40% of clasts >3 cm) (Schwarzkopf *et al.*, 2005). The crustal xenoliths are fragments enclosed in Merapi basaltic andesite and form a small proportion of the total erupted volume, which is estimated to be *c.* 2.5–4.3 km<sup>3</sup> for the 1998 deposits (Schwarzkopf *et al.*, 2005).

Samples of local crust were obtained for petrographic analysis from quarries south of Merapi at Sindet and Wunolelow and from a carbonate platform, which forms the cliffs at Parangtritis (Fig. 1). The units cropping out in quarries at Sindet and Wunolelow ~10 km south of Yogyakarta and 30 km south of Merapi are light grey to beige Miocene volcanic agglomerates of basaltic to andesitic composition inter-bedded with tuffaceous-marly clays. The source of the tephra and volcanoclastic units is probably the old Eocene to Miocene arc, whose eroded roots form the Southern Mountains Zone in Central and East Java (Smyth *et al.*, 2005). The volcanoclastic sediments are poorly sorted and are normally graded beds with sub-rounded lithic fragments and coarse rounded crystalline material (1–2 mm) at the base, and finer material toward the top (<0.2 mm). In thin section numerous Foraminifera types are visible in marly horizons, including unfragmented examples of *Globigerina*, *Cycloclpeus* and *Nummulites*. The cliffs (25–100 m) at Parangtritis are part of the Gunung Kidul, a plateau that runs along the southern coast of Central and East Java (Haryono & Day, 2004). This topographic high to the south of Merapi volcano is largely composed of Miocene carbonates of the Wonosari Formation, which consists of massive coral reef limestones in the south and bedded chalky limestones in the north (Balazs, 1968; van Bemmelen, 1949; Waltham *et al.*, 1983; Surono *et al.*, 1992). The total thickness of this unit is estimated to be >650 m and this platform is underlain by older Miocene volcanic and volcanoclastic rocks (Waltham *et al.*, 1983). The coral reef limestone is lithologically highly variable, but dominated by rudstones, packstones and framestones with interspersed lenses of volcanic ash (Waltham *et al.*, 1983). Samples taken from Parangtritis are massive limestones with numerous

biotherms of hexacorals and large Foraminifera including *Lepidocyclus* sp., *Miogyopsina* and *Flosculinella globulosa*.

### Whole-rock analyses

Selected samples were cut into cubes to remove weathered surfaces, and where obvious zoning was present xenolith samples were split into core and rim fractions. These samples were hand crushed in an agate mortar and pestle, sieved, and the resulting rock chips (0.5–0.7 mm) were hand picked using a binocular microscope. These chips were washed, dried, and then hand powdered using an agate mortar and pestle followed by a final phase of powdering in a ceramic teema© mill.

The mineralogy of whole-rock samples of powdered xenoliths was determined by X-ray diffraction (XRD) at the Facility for Earth and Environmental Analysis (FEEA), St. Andrews University (Scotland) using a PW1050 X-ray diffractometer with a fixed divergence slit and a graphite monochromator. Siemens Diffrac-AT software was used for identification of the unknown diffraction patterns in conjunction with the International Centre for Diffraction Data (ICDD) database, and quantification of multiple phases was carried out using Siroquant software (see <http://www.st-andrews.ac.uk/~acc/MAS.htm> for further details).

The powdered samples were dried at 105°C prior to analysis by X-ray fluorescence spectrometry (XRF) at the GEOMAR Research Centre, Germany. Fused glass beads were formed and analysed using an automated Phillips PW1480 X-ray spectrometer. All analyses were carried out using a Rh X-ray tube and calibrated to the international geological reference standards BHVO-1, JA-2, JB-2, JB-3 and JR-1. H<sub>2</sub>O and CO<sub>2</sub> were analysed on ignition of samples at 1200°C using a Rosemount CWA5003 IR photometer (see Troll & Schmincke, 2002). Standard analyses have been reported by Abratis *et al.* (2002).

Whole-rock Sr isotope analysis was carried out at the Danish Lithosphere Centre, Copenhagen, Denmark. From each sample, 200 mg was prepared in 15 ml beakers for whole-rock Sr isotope analysis and work was completed within a Class 10 Laminar Flow Hood with distilled acids used throughout the procedure. Samples were leached in HCl (6M) for 2 h to remove any alteration products and then thoroughly rinsed with Milli-Q water prior to acid digestion. JB-2 was used as the standard during the procedure, but was not acid leached prior to acid digestion. Samples, standards and blanks were then subjected to conventional HF–HNO<sub>3</sub>–HCl acid dissolution. Measurements of whole-rock Sr isotope ratios were conducted at the Geological Institute in Copenhagen by thermal ionization mass spectrometry (TIMS) using a VG Sector 54-IT system following the methods of Waight *et al.* (2002) (chemistry) and Bindeman *et al.* (2004) (analysis).

### Major element and Sr isotope microanalyses

*In situ* microanalyses of crystalline components were carried out using polished thick-sections (150 µm) of basaltic andesite clasts from the 1998 Merapi block-and-ash flow deposits and associated xenoliths. Major element analyses were carried out using the JEOL JXA-8200 Superprobe at the Geological Institute of Copenhagen, Denmark. A thin (20 nm) carbon coating was applied to selected thick sections (150 µm) prior to analysis to minimize charging. Analysis locations were selected using backscattered electron (BSE) images, allowing positioning accurate to ~1 µm. Samples were analysed for Si, Ti, Al, Fe, Mg, Ca, Na, K, Mn, Cr and Ni. To minimize Na loss, this element was analysed at the beginning of the sequence. Na counts were monitored during analysis, and remained stable over the measurement time. An electron beam of diameter of 2 µm and current of 15–30 nA was used with a count time of 30 s off peak and 30 s on peak. Relative analytical precision was < 1% for Si, Al and Ca, 2–3% for Na, < 10% for Fe and K, and ~20% for Mg and Ti.

Micro-sampling of crystal components for analysis of their Sr isotope ratios was performed at the Department of Earth Sciences, Durham University, UK, using a New Wave<sup>TM</sup> Micromill<sup>TM</sup> employing the techniques described by Charlier *et al.* (2006) and references therein. Analysis locations were selected using BSE images, and a binocular zoom microscope coupled with a linked computer workstation running specialist software that integrates the stage, mill and microscope optics and allows for precise location of the drill points reproducible to ±1 µm. The depth of the drill points was controlled using this setup; vertical movement is accommodated via movement in the microscope head–mill assembly reproducible to ±1 µm. Using tungsten carbide mill bits, multiple shallow points were milled along discrete zones in selected crystals. The number of drills per zone depended on the Sr ppm content of the feldspar, as a return of 3 ng of Sr was required for an analysis. Milling was carried out under a single drop of Milli-Q, which collected the drilled sample dust. This slurry was pipetted from the polished sample surface using disposable micropipettes and transferred directly to 3.5 ml screw-top beakers for processing and analysis. Procedural blanks were measured throughout the process by milling within a water droplet above the surface of the sample so that no grinding occurred. This blank was then pipetted and treated in an identical way to the samples. After processing, samples were analysed by TIMS using a Thermo-Finnigan Triton system, with average total procedural blanks between 12 ± 8 pg (2σ) and multiple analyses of NBS 987 averaging at 0.710261 ± 0.000017 (2σ) (*n* = 15) [within error of the value <sup>87</sup>Sr/<sup>86</sup>Sr = 0.710248 ± 0.000023 2σ (*n* = 427) reported by Thirlwall (1991)].

## RESULTS

Major element and Sr isotope variation in individual crystals from the Merapi basaltic andesite and metasedimentary xenoliths is illustrated in Figs 4–7 and in Tables 1 and 2. Mineralogical, whole-rock major element and Sr isotope data for selected xenolith samples are presented

in Fig. 3 and Tables 3–4, and as additional information in Figs 2 and 4–7.

### Mineralogy, petrology and geochemistry: basaltic andesite

The two main feldspar phenocryst compositions observed in the basaltic andesite are anorthite ( $An_{>90}$ ),

Table 1: Representative EMP feldspar analyses

Basaltic andesite								
	BA-101-C2	BA-101-C6	BA-159-C9	BA-159-C9	BA-101-C2	BA-101-C6	BA-159-C9	BA-159-C9
	rim	rim	rim	rim	core	core	core	core
<i>wt%</i>								
SiO <sub>2</sub>	55.73	55.90	57.73	51.95	45.98	44.77	45.44	45.46
TiO <sub>2</sub>	0.02	0.04	0.04	0.032	0.03	0.01	0.01	0.00
Al <sub>2</sub> O <sub>3</sub>	27.89	27.82	26.84	30.445	34.37	35.25	34.48	34.70
FeO	0.58	0.48	0.46	0.49	0.49	0.42	0.47	0.46
MgO	0.05	0.04	0.03	0.043	0.03	0.01	0.04	0.04
CaO	10.44	10.37	9.28	13.453	18.06	19.08	18.55	18.53
Na <sub>2</sub> O	5.30	5.48	6.03	3.775	1.32	0.71	1.02	0.98
K <sub>2</sub> O	0.41	0.45	0.59	0.246	0.06	0.02	0.05	0.04
Total	100.66	100.81	101.28	100.751	100.62	100.40	100.23	100.36
<i>mol%</i>								
Ab	46.74	47.61	52.23	33.20	11.67	6.30	8.99	8.68
An	50.86	49.85	44.40	65.38	87.97	93.56	90.73	91.10
Or	2.40	2.55	3.38	1.42	0.36	0.14	0.28	0.22
Calc-silicate								
	XCS-1C-C1	XCS-1C-C2	XCS-2-C1	XCS-2-C1	XCS-2-C2	XCS-2-C2	XCS-3-C1	XCS-3-C1
	core	core	rim	core	rim	core	core	core
<i>wt%</i>								
SiO <sub>2</sub>	44.20	43.42	53.31	44.20	46.11	42.51	42.90	43.47
TiO <sub>2</sub>	0.03	0.02	0.01	0.03	0.03	0.01	0.02	0.00
Al <sub>2</sub> O <sub>3</sub>	35.42	36.10	28.45	35.42	34.23	35.85	36.04	36.03
FeO	0.41	0.10	0.95	0.41	0.63	0.19	0.19	0.52
MgO	0.03	0.00	0.05	0.03	0.03	0.01	0.00	0.00
CaO	19.83	20.37	12.41	19.83	17.77	20.61	20.46	20.13
Na <sub>2</sub> O	0.37	0.03	4.27	0.37	1.30	0.00	0.02	0.08
K <sub>2</sub> O	0.00	0.00	0.39	0.00	0.05	0.00	0.00	0.01
Total	100.36	100.05	99.83	100.29	100.16	99.18	99.69	100.38
<i>mol%</i>								
Ab	3.24	0.30	37.52	3.24	11.66	0.00	0.17	0.69
An	96.76	99.70	60.25	96.76	88.02	99.98	99.81	99.27
Or	0.00	0.00	2.23	0.00	0.32	0.02	0.02	0.04

Basaltic andesite sample names: first number indicates the whole-rock sample followed by crystal number (e.g. 101-C6 is whole-rock 101, crystal C6).

characteristic of ultrabasic magmas and skarns, and labradorite ( $An_{50-70}$ ), which is more typical of basaltic to andesitic magmas (Fig. 4, Table 1) (Deer *et al.*, 1992). Individual crystals show variations in the mole fraction of anorthite from  $An_{34}$  to  $An_{95}$  (Figs 4 and 5). Major element core-to-rim variation is observed in all of the analysed feldspar phenocrysts, with both normal- and reverse-zoned crystals present (Fig. 5). However, high-anorthite feldspar is generally confined to the cores of large crystals, with lower An mol% compositions more common in crystal rims. Transitions between zones are typically sharp and are often marked by resorption surfaces with distinct shifts in

*Table 2: Crystal-isotope stratigraphy Sr ratios for plagioclase in Merapi 1998 basaltic andesite block-and-ash flow eruptive products*

Sample, location	$^{87}\text{Sr}/^{86}\text{Sr}$	2SD
<i>BA-101-C2, basaltic andesite</i>		
1, core	0.705699	0.000016
2, inner zone	0.705688	0.000016
3, outer zone	0.705743	0.000011
4, rim	0.705795	0.000019
<i>159-C9, basaltic andesite</i>		
1, core	0.705841	0.000014
2, inner zone	0.706277	0.000012
3, rim	0.705769	0.000013
<i>159-C3, basaltic andesite</i>		
1, core	0.705846	0.000014
2, inner zone	0.705854	0.000017
3, mid zone	0.705992	0.000013
4, outer zone	0.705902	0.000020
5, rim	0.705807	0.000015
<i>101-C6, basaltic andesite</i>		
1, core	0.705845	0.000017
2, inner zone	0.705682	0.000006
3, outer zone	0.705712	0.000006
4, rim	0.705813	0.000009
<i>159-GM, basaltic andesite</i>		
Groundmass	0.705812	0.000018
Groundmass	0.705912	0.000028
<i>XCS-102</i>		
C1	0.706018	0.000052
<i>Calc-silicate xenolith</i>		
C2	0.705985	0.000023

Location numbers correlate to zones sampled, illustrated in Fig. 6.

An content of up to 40 mol% between zones (Fig. 5). For a basaltic andesite melt fractionating plagioclase, pyroxene, Fe–Ti oxides and amphibole and/or experiencing mixing with a more differentiated or more mafic magma, a positive correlation between An mol%, MgO wt% and FeO wt% is expected (Bindeman *et al.*, 1998; Troll & Schmincke, 2002; Ginibre *et al.*, 2002). However, the analysed crystals appear to show an anticorrelation between An content and wt% MgO or FeO (Fig. 5a and b) and for the majority of analysed compositions, high An mol% feldspar (> 80 mol%), have low MgO and FeO contents (Fig. 5c).

Core-to-rim variations in  $^{87}\text{Sr}/^{86}\text{Sr}$  are observed in all samples (Fig. 6, Table 2) and the range in  $^{87}\text{Sr}/^{86}\text{Sr}$  for plagioclase phenocrysts (0.70568–0.70627) markedly exceeds that recorded in whole-rocks from recent Merapi block-and-ash flows (0.70571–0.70574; Gertisser & Keller, 2003a; Fig. 7). The most radiogenic  $^{87}\text{Sr}/^{86}\text{Sr}$  ratio obtained from the sampled crystals was from a zone with a high An content of ~90 mol% (Fig. 6b). Radiogenic  $^{87}\text{Sr}/^{86}\text{Sr}$  ( $\geq 0.70590$ ) is coupled with an An content of >90 mol%, whereas lower  $^{87}\text{Sr}/^{86}\text{Sr}$  ( $\leq 0.70585$ ) is coupled with an An of 40–60 mol% in three of the four phenocrysts analysed in this study. One of the analysed crystals (Fig. 6a) shows a more restricted range in  $^{87}\text{Sr}/^{86}\text{Sr}$  with a smaller range in An mol% and lacks extreme dissolution surfaces. The outer crystal rims of all the analysed crystals are in equilibrium with the groundmass ( $^{87}\text{Sr}/^{86}\text{Sr}$  of 0.70581–0.70591). The groundmass also exceeds the  $^{87}\text{Sr}/^{86}\text{Sr}$  isotope range defined for whole-rock analyses of recent Merapi block-and-ash flow deposits (Figs 6 and 7), and feldspar in the inner zones and cores is typically in Sr isotopic disequilibrium with the analysed groundmass (Fig. 6).

### Petrology and geochemistry: metasedimentary xenoliths

Xenoliths hosted in Merapi magmas may be subdivided into two main types: calc-silicate skarns (Fig. 2a and b; Table 4, XCS-1, XCS-3, XCS-7, XCS-9), and less common, more silicic, metamorphosed, volcanoclastic sediments (Fig. 2c and d, Table 4; XCS-2, XCS-4).

The calc-silicate xenoliths have a characteristic skarn-type mineralogy of wollastonite and diopside, with lesser amounts of plagioclase, quartz, tremolite, and rare garnet and opaques in some of the samples, identified both petrographically and by XRD analysis (Fig. 2, Table 3). The relative abundance of these minerals fluctuates from sample to sample and is likely to be a function of heterogeneity in the original protolith, potentially a carbonate of variable purity, and due to degree of interaction with the host andesite. Variability in the protolith and degree of metamorphism also appear to be responsible for the spread in data for more silicic metamorphosed volcanoclastic sediments. These samples occasionally possess primary sedimentary structures including laminations

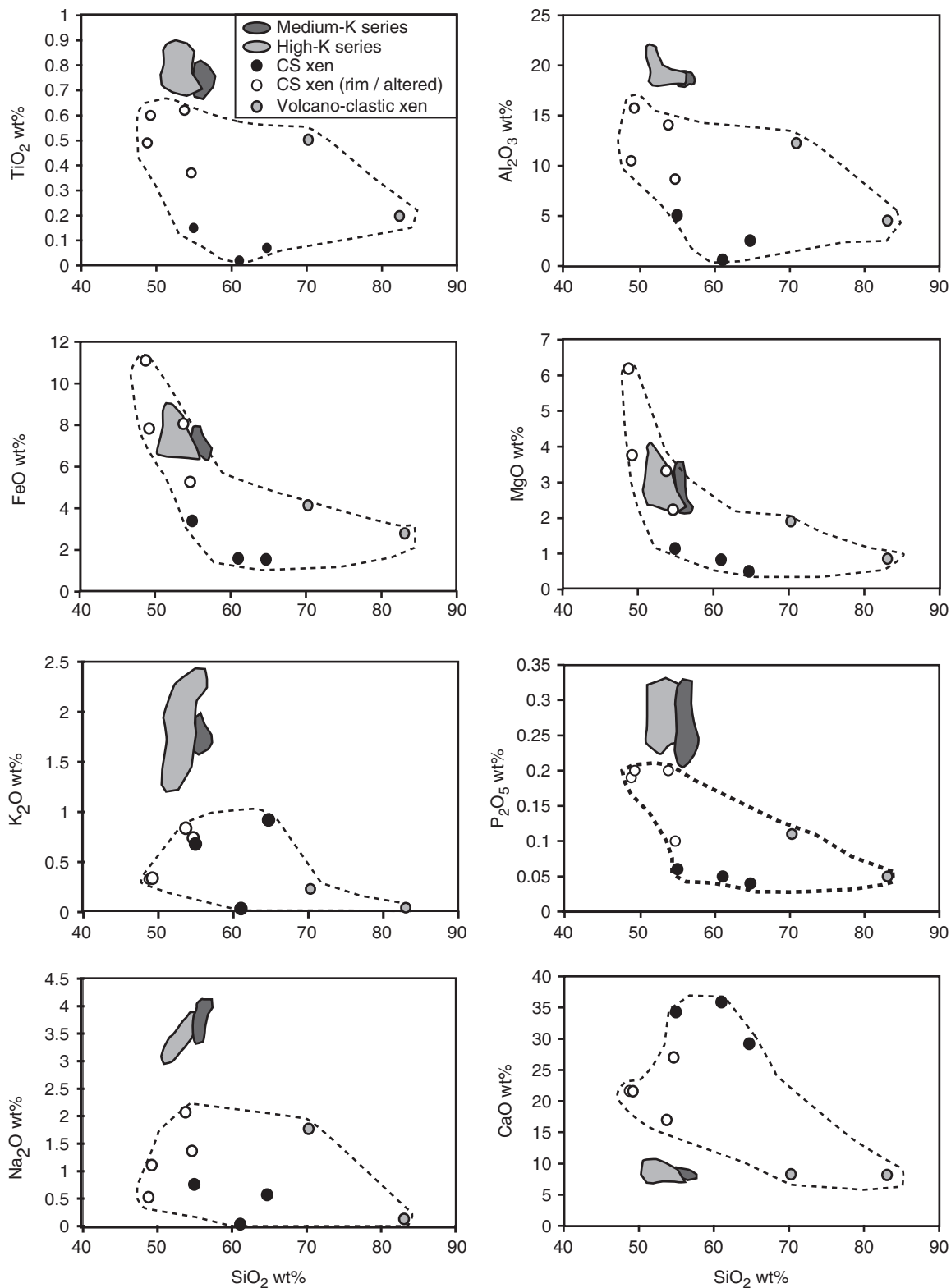
Table 3: Xenolith rock type, textural features and mineralogy

Deposit	Sample	Rock type	Type	Grain size	Mineralogy (relative vol.%)						
					Wo	An	Di	Trm	Qtz	Gros	Opaque
1998 BAF	XCS-1R	Calc-silicate xen	xen rim	fine	6	30	60	2	1	0	1
1998 BAF	XCS-1C	Calc-silicate xen	xen core	medium	70	5	7	0	18	0	0
1998 BAF	XCS-2	Volcano-clastic xen	xen wr	fine/medium	3	50	10	0	34	0	3
1998 BAF	XCS-3	Calc-silicate xen	xen wr	medium	70	10	3	0	10	5	2
1998 BAF	XCS-4	Volcano-clastic xen	xen wr	fine/medium	5	15	11	0	67	0	2
1998 BAF	XCS-7R	Calc-silicate xen	xen rim	fine	57	24	16	0	0	0	3
1998 BAF	XCS-7T	Calc-silicate xen	xen trans	fine	11	67	22	0	0	0	0
1998 BAF	XCS-7C	Calc-silicate xen	xen core	medium	47	37	16	0	0	0	0
1998 BAF	XCS-9	Calc-silicate xen	xen wr	medium	32	47	20	0	0	0	1

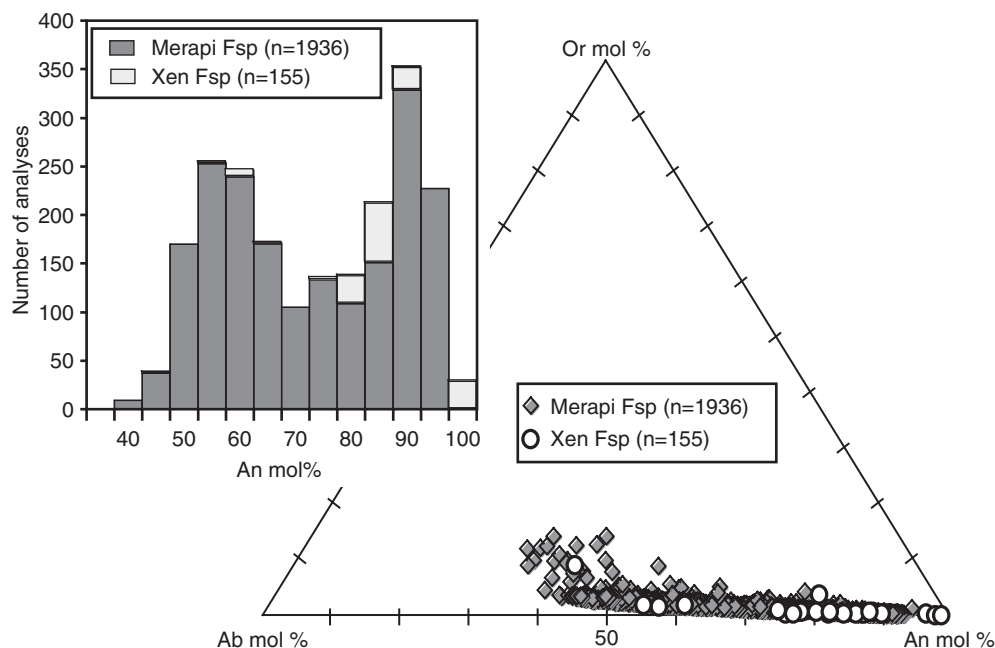
BAF, basaltic andesite block-and-ash flow; xen rim, xenolith rim; xen core, xenolith core; xen wr, xenolith whole rock; xen trans, transition zone from core to rim. Wo, wollastonite; An, anorthite; Di, diopside; Trm, tremolite; Qtz, quartz; Gros, grossular. Average grain size: coarse >5 mm; medium 1-5 mm; fine <1 mm.

Table 4: Whole-rock major element, trace element (XRF) and Sr isotope (TIMS) data for xenoliths

Sample:	XCS-1R	XCS-1C	XCS-3	XCS-2	XCS-4	XCS-7R	XCS-7T	XCS-7C	XCS-9
Type:	xen rim	xen core	xen wr	xen wr	xen wr	xen rim	xen trans	xen core	xen wr
<i>wt%</i>									
SiO <sub>2</sub>	48.76	61.02	64.70	70.27	83.07	53.74	54.64	54.93	49.21
TiO <sub>2</sub>	0.49	0.02	0.07	0.51	0.51	0.62	0.37	0.15	0.60
Al <sub>2</sub> O <sub>3</sub>	10.48	0.61	2.52	12.50	4.51	14.07	8.67	5.06	15.75
Fe <sub>2</sub> O <sub>3</sub>	11.10	1.59	1.55	4.14	2.79	8.07	5.27	3.40	7.83
MnO	0.34	0.22	0.27	0.11	0.11	0.26	0.28	0.29	0.23
MgO	6.19	0.83	0.51	1.91	0.86	3.32	2.23	1.15	3.76
CaO	21.62	35.88	29.18	8.27	8.19	16.96	27.02	34.29	21.61
Na <sub>2</sub> O	0.53	0.01	0.57	1.77	0.13	2.07	1.37	0.76	1.11
K <sub>2</sub> O	0.33	0.01	0.92	0.23	0.02	0.84	0.74	0.68	0.34
P <sub>2</sub> O <sub>5</sub>	0.19	0.05	0.04	0.11	0.05	0.20	0.10	0.06	0.20
<i>ppm</i>									
Co	114	43	53	56	59	59	50	42	65
Cr	43	18	18	96	644	71	36	18	18
Ni	18	2	2	4	8	21	8	2	6
V	91	12	12	72	44	138	80	22	114
Zn	108	16	26	48	54	101	70	41	97
Ce	10	10	10	29	31	42	10	25	24
La	14	14	14	14	14	14	14	14	14
Nb	2	2	2	2	2	5	2	2	3
Ga	13	8	8	13	8	15	8	8	15
Pb	4	4	4	8	5	6	4	8	6
Pr	5	4	4	4	4	4	4	4	4
Rb	11	4	27	6	4	22	21	21	11
Ba	63	8	43	234	184	243	199	102	122
Sr	710	425	66	359	171	424	319	235	442
Th	4	5	5	4	5	4	5	8	7
Y	18	21	7	24	35	19	18	15	29
Zr	93	13	25	100	238	94	70	49	127
Total	100.21	100.29	100.38	99.95	100.42	100.32	100.82	100.84	100.75
<sup>87</sup> Sr/ <sup>86</sup> Sr	0.707655	0.707866	0.705842		0.707361				
2SD	0.00006	0.00002	0.00002		0.00002				



**Fig. 3.** Major element variations in the xenoliths relative to the Merapi basaltic andesites (Gertisser & Keller, 2003a). The xenolith samples show significant geochemical variation, particularly in  $\text{SiO}_2$ . Volcano-clastic xenoliths, calc-silicate xenolith rims (CS xen) and strongly metamorphosed calc-silicate xenoliths are highlighted. A transition from calc-silicate xenolith interiors to more magmatic signatures at the exterior is evident (e.g. FeO and MgO).



**Fig. 4.** Triangular An–Ab–Or plot of all Merapi basaltic andesite ( $n = 1936$ ) and xenolith feldspars ( $n = 155$ ) analysed in this study. Inset shows histogram of plagioclase composition in basaltic andesites and xenoliths. Plagioclase from the basaltic andesite shows a bimodal distribution, whereas xenolith feldspar has a more restricted unimodal composition towards high An mol% (only four analyses have  $An_{<70}$ ).

and grading present as alternating bands of medium to fine grain size with variable mineralogy (Fig. 2). Commonly, these primary sedimentary textures are thermally overprinted. Alternating layers composed primarily of quartz and plagioclase or plagioclase and diopside are most common, with rare zircon and titanomagnetite present as small (0.05 mm) grains.

Plagioclase crystals in both xenolith types are typically euhedral laths (Fig. 2); these can be normally zoned and exhibit a significant range in composition from anorthite to andesine, with feldspars in the calc-silicate xenoliths typically restricted to values between 80 and 100 An mol% (Fig. 4, Table 1). The major element compositions of the calc-silicate feldspars are similar to the high-CaO, low-MgO, low-FeO cores in many of the magma-hosted plagioclase crystals (Figs 4 and 5, Table 2). Notably, the  $^{87}\text{Sr}/^{86}\text{Sr}$  ratios of these xenolith-hosted plagioclase crystals (0.70598–0.70602) overlap with the  $^{87}\text{Sr}/^{86}\text{Sr}$  range observed in the high  $^{87}\text{Sr}/^{86}\text{Sr}$ , high-An, low-MgO, low-FeO plagioclase crystal cores in the basaltic andesite (Figs 6 and 7, Table 2).

As well as geochemical variation being present on a single-crystal scale, there is also zoning evident on a hand-sample scale (Fig. 3, Table 3). Many of the calc-silicate xenoliths possess strong reaction rims at their margins and where the host basaltic andesite magma has infiltrated the less affected cores. The reaction rims can be several centimetres in width and are marked by an

increase in diopside, anorthite and oxides such as titanomagnetite (Figs 2 and 3). There is an increase in the amount of wollastonite towards the cores of these xenoliths (up to 70%) (Fig. 2, Table 3). The distinct rims, present in several of these xenoliths, have mineral assemblages and whole-rock major element signatures that are closer to magmatic signatures than are those of the cores, with elevated Fe, Mg, Ti and Al, indicating significant interaction with the host basaltic andesite (Fig. 3, Table 3–4). The more silicic xenoliths also possess reaction rims; however, they are not as strongly developed (< 0.5 cm diameter) as those observed in the calc-silicate xenoliths (Fig. 2).

## DISCUSSION

Inter-crystal  $^{87}\text{Sr}/^{86}\text{Sr}$  heterogeneity of plagioclase is thought to be associated with processes such as magma mixing and crustal assimilation (Davidson & Tepley, 1997; Ramos *et al.*, 2005). A geochemical profile for a plagioclase crystal growing undisturbed in a primary magma experiencing assimilation of a more silicic crustal material (e.g. assimilation–fractional crystallization; AFC) would show increasing  $^{87}\text{Sr}/^{86}\text{Sr}$  with decreasing An mol%, MgO wt% and FeO wt% from the crystal core outwards. In the case of mafic magma replenishment with less contaminated magma, or introduction of xenocrysts sourced from a more mafic magma or lithology, the converse

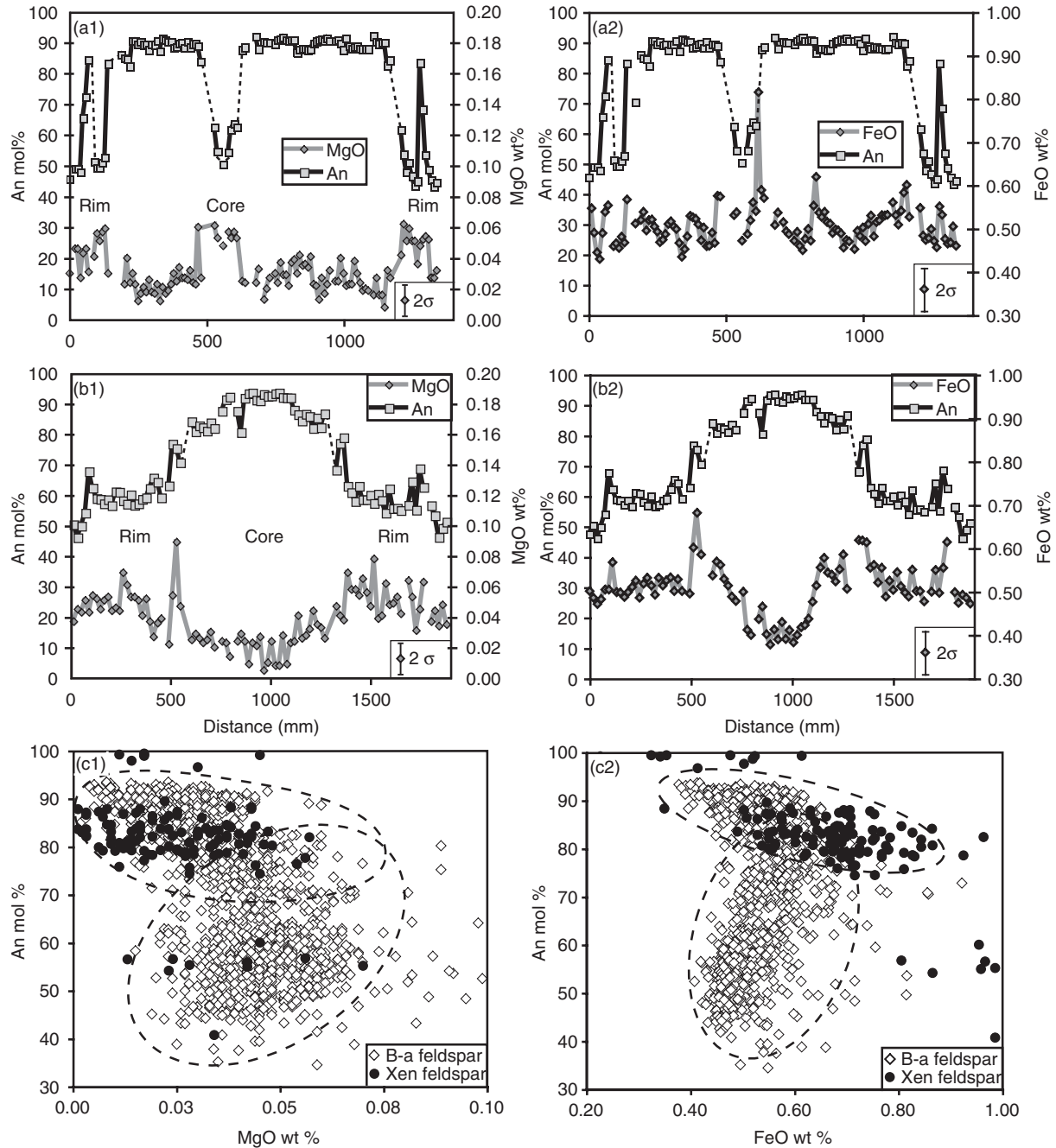


**Fig. 5.** An mol% profiles plotted relative to MgO wt% (a1 and b1) and FeO wt% (a2 and b2) profiles for normally zoned (a) and reverse zoned (b) plagioclase crystals from Merapi basaltic andesite. Sharp jumps in An content of up to 40 mol% reflect major changes in growth conditions and are located near dissolution surfaces. An mol% content is negatively correlated with MgO wt% and FeO wt%. (c) A plot of all analyses of basaltic andesite (B-a feldspar,  $n = 1936$ ) and xenolith feldspar (Xen. feldspar,  $n = 155$ ), indicating that negative correlation exists for An compositions of  $>85$  mol% and a positive correlation for An compositions of  $<85$  mol%. Dashed ellipses highlight the two trends for MgO wt% (c1) and FeO wt% (c2).

would be the case (Davidson & Tepley, 1997). The former appears to be a likely hypothesis for one of the plagioclase phenocrysts analysed for Sr isotopes (Fig. 6a). However, simple magma mixing, mafic replenishment or AFC

processes cannot explain the profiles observed in the other crystals analysed. Feldspar with the highest An mol% typically has the most radiogenic  $^{87}\text{Sr}/^{86}\text{Sr}$  (Fig. 6b–d) and a negative correlation with MgO wt% and FeO wt%

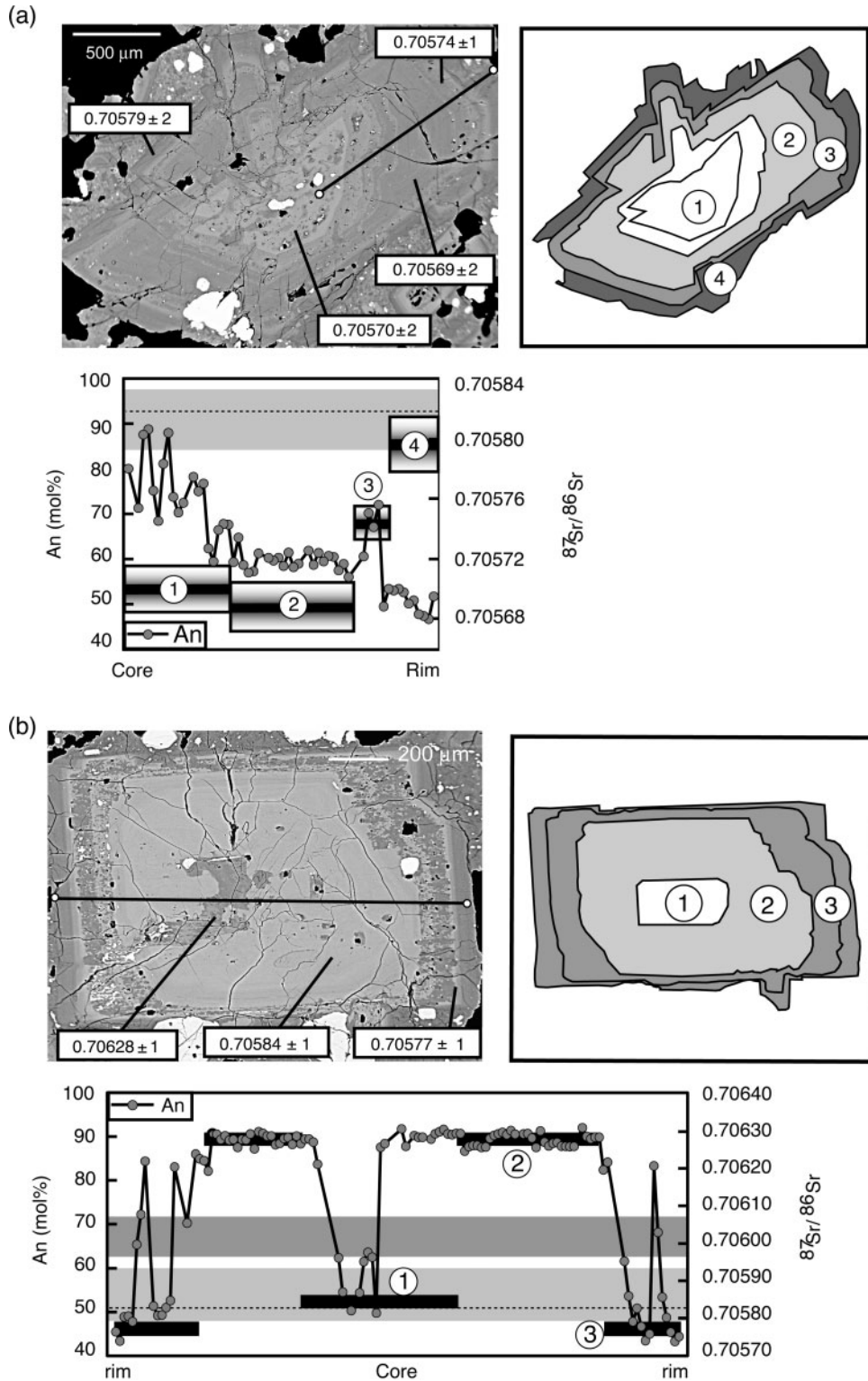


**Fig. 6.**  $^{87}\text{Sr}/^{86}\text{Sr}$  and An mol% zoning profiles for plagioclase phenocrysts (a–d) in comparison with groundmass (light grey bar) and plagioclase from a metamorphosed sedimentary xenolith (dark grey bar). Lower limit of  $^{87}\text{Sr}/^{86}\text{Sr}$  ratios for xenolith whole-rock analyses delimited by dashed line. The rectangles represent  $^{87}\text{Sr}/^{86}\text{Sr}$  ratios (right axis) and the length and height of these bars corresponds to the drilled area and analytical error ( $2\sigma$ ), respectively. Back-scattered electron images illustrate zoning patterns and locations of electron microprobe traverses (with multi part traverses labelled a and b). Circled numbers correspond to drilled zones listed in Table 2. (See text for details.)

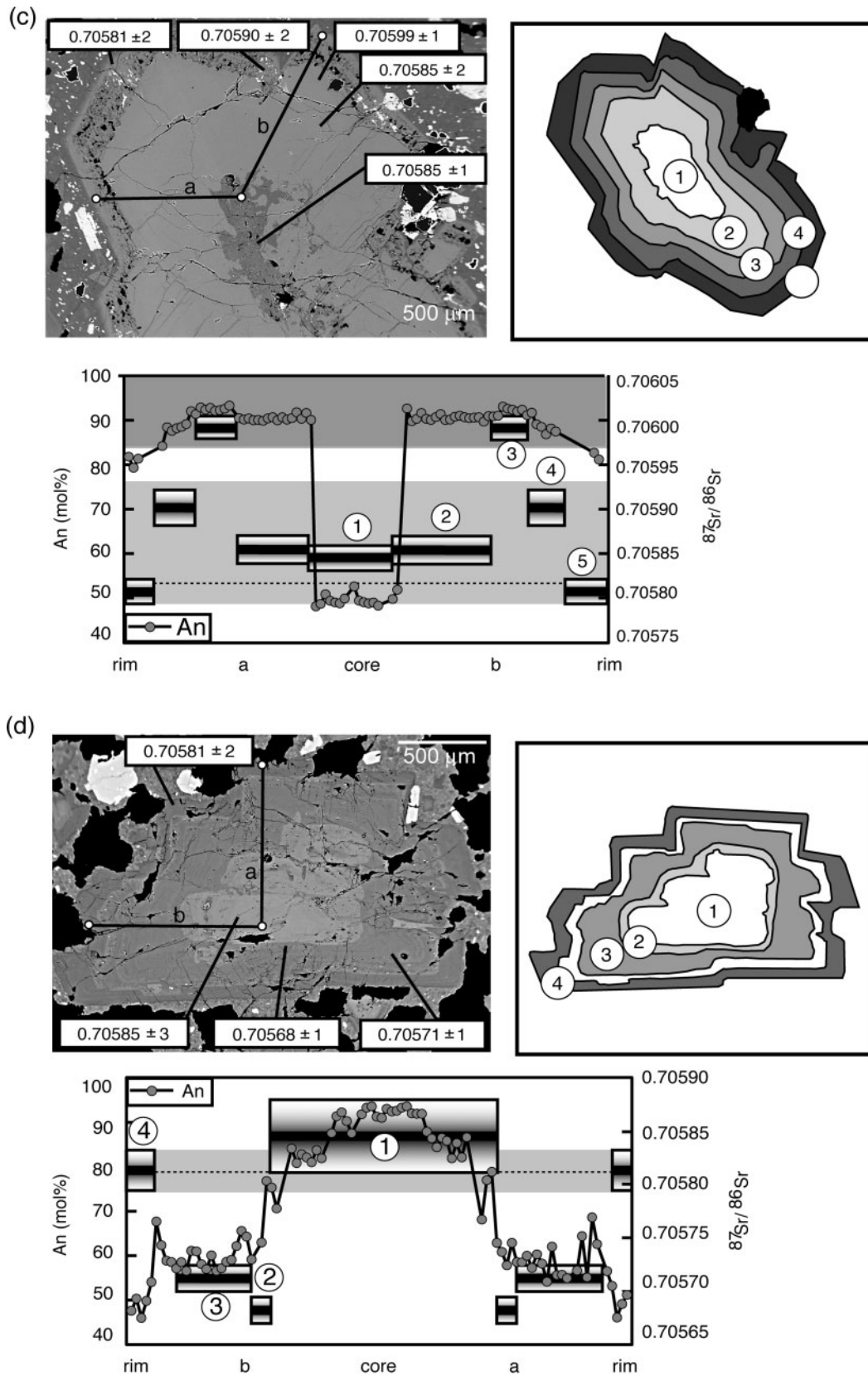
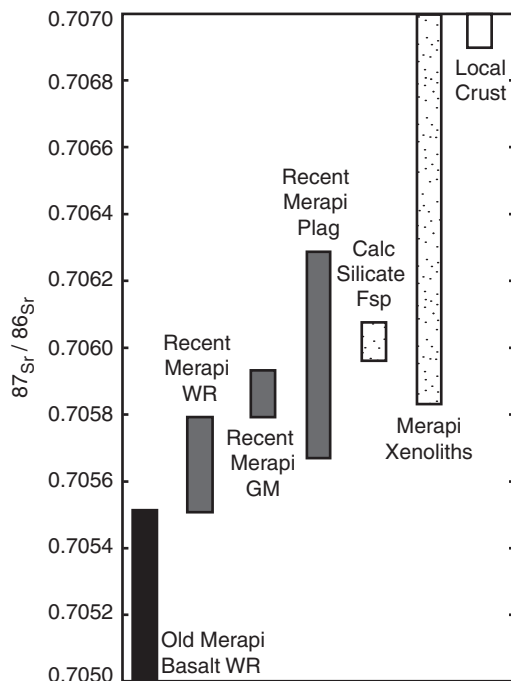


Fig. 6. Continued



**Fig. 7.**  $^{87}\text{Sr}/^{86}\text{Sr}$  values for recent Merapi feldspar, groundmass (GM) and xenoliths plotted relative to a local carbonate crust sample, host basaltic andesite, and Holocene basalts taken from Gertisser & Keller (2003a).

(Fig. 5). The lower  $^{87}\text{Sr}/^{86}\text{Sr}$  ratios in the cores of two of the plagioclase crystals (Fig. 6b and c) appear to be a late internal dissolution effect that has been developed simultaneously with the rim. This is evident by the corresponding geochemical signatures and the patchy replacement texture present; a channel from the exterior to the interior of the crystal is visible in Fig. 6c. Fluctuations in the An content of plagioclase can result from variation in a number of physical factors including melt temperature, pressure and the water content of the magma (e.g. Duncan & Green, 1987; Beard & Borgia, 1989; Housh & Luhr, 1991; Sisson & Grove, 1993). However, the marked variation in An mol% present in the analysed crystals, coupled with the variation in Sr isotope ratios, requires the action of open-system processes rather than changes in physical parameters. A xenocrystic origin for these high An mol%, high radiogenic Sr crystal cores (Fig. 6b–d) is therefore considered likely, given their strong similarities to the feldspar hosted in the metasedimentary xenoliths (Figs 4–6).

The metasedimentary xenoliths found throughout the recent pyroclastic deposits (Fig. 2) indicate contact metamorphism between country rock and Merapi magmas in the mid- to upper crust (Camus *et al.*, 2000). The presence of wollastonite in the calc-silicate xenoliths is evidence for a reaction of Ca-rich carbonate with basaltic andesitic magma at temperatures  $>600^\circ\text{C}$  ( $\text{CaCO}_3 + \text{SiO}_2 \rightarrow \text{CaSiO}_3 + \text{CO}_2$ ; Bowen, 1940; Tracey

& Frost, 1991; Deer *et al.*, 1992). Wollastonite is unstable below  $400^\circ\text{C}$  (Milke & Metz, 2002) and the dominance of this mineral along with anorthite and diopside in these xenoliths, coupled with limited occurrence of lower-grade assemblages (e.g. tremolite and quartz), indicates relatively rapid cooling following their formation. The likely protoliths for these xenoliths are the Cenozoic carbonate and volcanoclastic lithologies present in the Kendeng basin, with a maximum thickness of 11 km (Smyth *et al.* 2005), and/or the Cenozoic carbonates, marls, and volcanic rocks of the Southern Mountain zone. There is limited information on the physical characteristics of the Merapi magma plumbing system. However, there is evidence that the bulk of magma storage is sited in the mid- to lower crust (Westerhaus *et al.*, 1998; Beauducel & Cornet, 1999; Ratdomopurbo & Poupinet, 2000; Gertisser, 2001; Gertisser & Keller, 2003b; Chadwick *et al.*, in preparation),  $>5$  km below sea level. This indicates that these reactions probably occurred in the mid-crust under significant heat and pressure (between 6 and 11 km).

The calc-silicate and volcanoclastic xenolith whole-rock geochemistry confirms interaction with the host andesite and the reaction process between country rock and magma is evident in their mineralogy and major element composition. Several calc-silicate samples show a dominance of wollastonite in the core and an increasingly magmatic signature (Fig. 3, Table 4) with a dominance of anorthite and diopside towards the rim (Table 3). Bulk compositions thus in part represent the final product of an exchange of material between the xenoliths and Merapi magma. Taking a recent Merapi magma that is relatively undifferentiated with respect to  $\text{SiO}_2$  and  $\text{MgO}$  (51.85 wt%  $\text{SiO}_2$ , 18.53 wt%  $\text{Al}_2\text{O}_3$ , 8.6 wt%  $\text{Fe}_2\text{O}_3$ , 3.9 wt%  $\text{MgO}$  and 9.58 wt%  $\text{CaO}$ ; Gertisser & Keller, 2003a), the chemical potential contrast between this magma and metasedimentary xenoliths depends on the exact composition of the original sedimentary protolith. However, using the compositions of the xenoliths themselves, significant contrasts for Si, Al, Ca, Mg and potentially Fe are probable. Thus, the xenoliths may have gained Al, Ti, Fe and Mg (supported by the occurrence of titanomagnetite almost exclusively in the reaction rims of the calc-silicate xenoliths), with variable transfer of Si and Ca depending on starting composition. This transfer could have been achieved by direct melting and mixing of fusible components or by fluid interaction with encompassing Merapi magmas. Vesicular textures at lava–xenolith interfaces indicate intense fluid interaction, potentially as a result of  $\text{CO}_2$  release (Troll *et al.*, 2003, fig. 2), and metasomatic alteration is typical in the formation of skarns (Barton *et al.*, 1991).

The overlap between the geochemical characteristics of the anorthite present in the xenolith rims and the high-An regions of some zoned phenocrysts suggests that this

Table 5: EC–AFC parameters used for quantitative modelling of Sr isotopic variations at Merapi volcano

	Compositional parameters (curves in Fig. 6a)				Thermal parameters	
	XCS-1r	XCS-1c	XCS-3	XCS-4		
Element	Sr (ppm)	Sr (ppm)	Sr (ppm)	Sr (ppm)	t <sub>lm</sub>	1280°C
Magma: conc.	595	595	595	595	t <sub>m0</sub>	1280°C
Bulk $D_0$	1	1	1.5	1.5	t <sub>la</sub>	1000°C
Assimilant: conc.	710	434	66	154	t <sub>a0</sub>	700°C
Bulk $D_0$	0.7	0.7	0.7	1	t <sub>s</sub>	800°C
Isotope	$^{87}\text{Sr}/^{86}\text{Sr}$	$^{87}\text{Sr}/^{86}\text{Sr}$	$^{87}\text{Sr}/^{86}\text{Sr}$	$^{87}\text{Sr}/^{86}\text{Sr}$	c <sub>pm</sub>	1484 J/kg K
Ratio magma	0.70554	0.70554	0.70554	0.70554	c <sub>pa</sub>	1370 J/kg K
Ratio assimilant	0.70765	0.70787	0.70584	0.70736	h <sub>cry</sub>	396000 J/kg
					h <sub>fus</sub>	250000 J/kg

	Compositional parameters (curves in Fig. 6b)				Thermal parameters	
	Crust 1a	Crust 1b	Crust 1c	Crust 1d		
Element	Sr	Sr	Sr	Sr	t <sub>lm</sub>	1280°C
Magma: conc.	595	595	595	595	t <sub>m0</sub>	1280°C
Bulk $D_0$	1	1	1	1	t <sub>la</sub>	1000°C
Assimilant: conc.	1000	500	1000	500	t <sub>a0</sub>	700°C
Bulk $D_0$	0.7	0.7	0.7	0.7	t <sub>s</sub>	800°C
Isotope	$^{87}\text{Sr}/^{86}\text{Sr}$	$^{87}\text{Sr}/^{86}\text{Sr}$	$^{87}\text{Sr}/^{86}\text{Sr}$	$^{87}\text{Sr}/^{86}\text{Sr}$	c <sub>pm</sub>	1484 J/kg K
Ratio magma	0.70554	0.70554	0.70554	0.70554	c <sub>pa</sub>	1370 J/kg K
Ratio assimilant	0.70735	0.70735	0.70693	0.70693	h <sub>cry</sub>	396000 J/kg
					h <sub>fus</sub>	250000 J/kg

Terminology from Spera & Bohrsen (2001): t<sub>lm</sub>, liquidus of magma; t<sub>m0</sub>, initial temperature of magma; t<sub>la</sub>, liquidus of assimilant; t<sub>a0</sub>, initial temperature of assimilant; t<sub>s</sub>, solidus temperature; c<sub>pm</sub>, magma isobaric specific heat capacity; c<sub>pa</sub>, assimilant isobaric specific heat capacity; h<sub>cry</sub>, enthalpy of crystallization; h<sub>fus</sub>, enthalpy of fusion.

feldspar is probably the equivalent of the high  $^{87}\text{Sr}/^{86}\text{Sr}$ , high-An, low-Mg, low-Fe plagioclase in the basaltic andesite lavas. These crystal cores formed via a complex contact metamorphic–metasomatic process from a sedimentary protolith, which thus accounts for the apparent decoupling between An mol% and MgO wt% and FeO wt%, together with relatively highly radiogenic Sr. Several previous studies have addressed limestone assimilation by mafic magmas (e.g. Tilley, 1952; Joesten, 1977; Baker & Black, 1980; Joesten *et al.*, 1994; Owens, 2000). In these studies, changes were noted in the chemical composition and mineralogy of the mafic magma, including resorption of primary igneous minerals such as olivine and the crystallization of Ca–Al-rich phases such as plagioclase and clinopyroxene. In these studies, calc-silicate minerals such as wollastonite and grossular and lesser anorthite are envisaged to form at or near the magma–crust/xenolith interface.

### Quantitative modelling of crustal interaction

Considering the  $^{87}\text{Sr}/^{86}\text{Sr}$  range for the Merapi system as a whole, both groundmass and crystal Sr isotope ratios exceed the range seen in the whole-rocks. Rather than a source process, this indicates significant late-stage contamination in the crust given the stability field of plagioclase (Ramos *et al.*, 2005), which is obscured in whole-rock isotope ratios. Heterogeneous groundmass and melt inclusions as reported by Schwarzkopf *et al.* (2001), as well as small basaltic inclusions (Troll *et al.*, 2003) incorporated into whole-rocks, are likely to result in generally suppressed  $^{87}\text{Sr}/^{86}\text{Sr}$  whole-rock values. Extensive evidence of magma mixing and mafic replenishment is apparent in recent Merapi whole-rocks (Gertisser & Keller, 2003b; Troll *et al.*, 2003; Chadwick *et al.*, in preparation); and previous workers have argued for the process of magma mixing during recent eruptions (Boudon *et al.*, 1993;

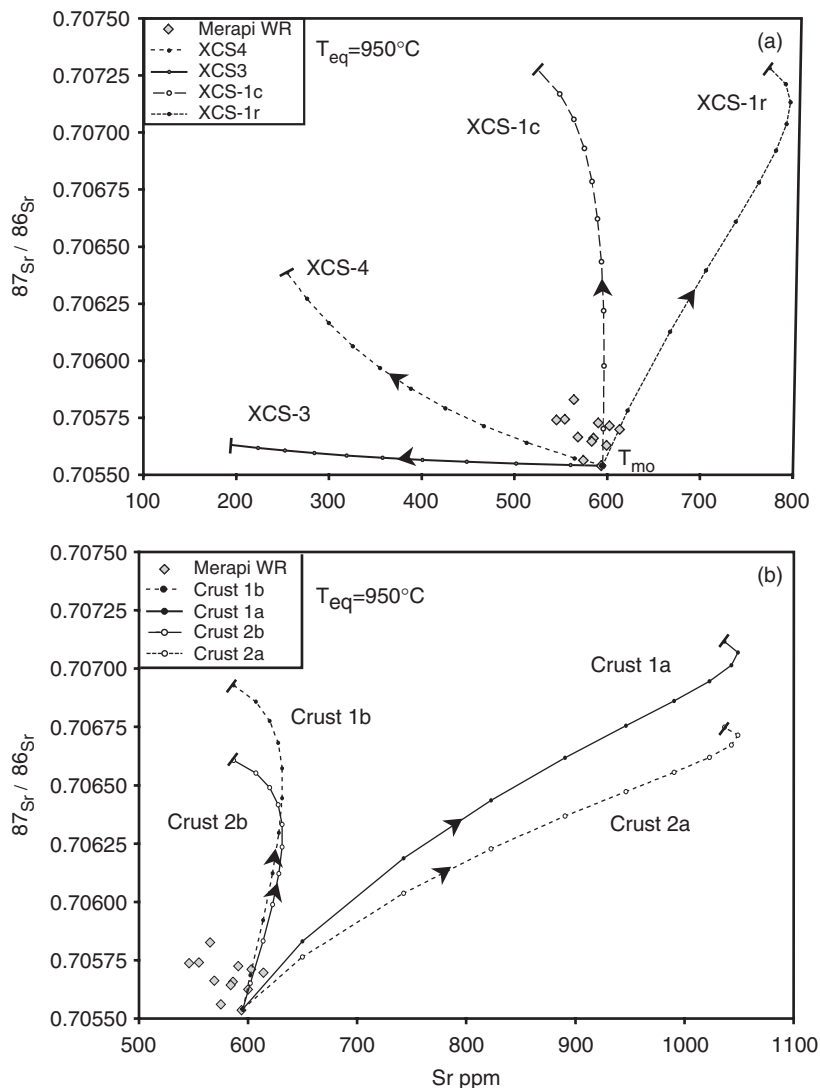


**Fig. 8.** Sr ppm vs  $^{87}\text{Sr}/^{86}\text{Sr}$  data for recent Merapi basaltic andesite (Gertisser & Keller, 2003a), Central Java crust, Merapi xenoliths and results from EC-AFC modelling (Bohrson & Spera, 2001; Spera & Bohrson, 2001) with parameters used listed in Table 5. Arrows indicate direction of falling magma temperature ( $T_m$ ) and each symbol on EC-AFC curve represents a normalized temperature increment of 0.01 ( $\sim 15^\circ\text{C}$ ). (a) Models using xenoliths compositions as assimilants encompass the Merapi basaltic andesite data field. (b) Models using Javan carbonate crust as assimilant do not account for the entire range observed in recent Merapi basaltic andesite.

Camus *et al.*, 2000). This mixing is likely to buffer  $^{87}\text{Sr}/^{86}\text{Sr}$  ratios for the system as represented by the whole-rock analyses.

Despite representing an averaged composition of a heterogeneous mass of crystals and mixed melts, whole-rock analyses of recent Merapi basaltic andesite and potential crustal assimilants (xenoliths and country rock) were used to model crustal process using the energy constrained assimilation and fractional crystallization (EC-AFC) model of Spera & Bohrson (2001). Thermal and geochemical parameters are listed in Table 5 and results plotted in Fig. 8.

We have produced models for two situations. The first model consists of a reservoir in which fractionating

mafic Merapi magma is contaminated by heterogeneous thermally altered country rocks (as represented by the calcareous and volcanoclastic xenoliths; Fig. 8a). The xenolith inclusions were used given the lack of sufficient data for Central Java crustal lithologies. The second model incorporates contamination of Merapi magmas by carbonate crust as represented by a crustal sample from the Wonosari Formation (Fig. 8b).

In our simulations, melt temperature was assumed to be  $1200^\circ\text{C}$  ( $T_{lm}=T_{m0}$ ) based on petrochemical data (Gertisser, 2001). A temperature of  $700^\circ\text{C}$  ( $T_{a0}$ ) was assigned to the Merapi basement, consistent with mid-crustal magma storage and geophysical data suggesting a high heat flux in Central Java and the area beneath

Merapi volcano (Wagner *et al.*, 2007; Chadwick *et al.*, in preparation; Koullakou *et al.*, 2007). The liquidus temperature of the crustal rocks ( $T_{1a}$ ) is assumed to be 1000°C based on experimental studies (Joesten *et al.*, 1994; Lentz, 1999; Owens, 2000; Wenzel *et al.*, 2001, 2002) and the solidus  $T$  of the magma is 800°C ( $T_s$ ). Sr is assumed to be mildly incompatible to compatible in the assimilants (bulk  $D_o$  of 0.7–1) depending on composition (e.g. Barnes *et al.*, 2005), and compatible in the magma given the dominance of plagioclase (bulk  $D_o$  of 1). The model requires the definition of the equilibration temperature ( $T_{eq}$ ), which describes the approach of the system to equilibrium during the process of heat exchange, and is equal to or higher than eruptive temperature (Spera & Bohrsen, 2001). An equilibration temperature of 950°C is used in the models.

The calculated EC-AFC curves represent the geochemical paths simulated by interaction between a recent Merapi magma and a heterogeneous Javan crust as represented by xenoliths and Wonosari Limestone. These models indicate that contamination of this Merapi magma with 0.08–0.4 mass of assimilated melt with 40–50% crystallization replicates the full range in Sr isotope ratios observed in recent Merapi eruptive rocks [ $<1900$  C<sup>14</sup> years BP, after Gertisser & Keller (2003b)]. The curves modelled using xenolith compositions as assimilant suggest that multiple crustal sources contribute to the range in Sr isotope compositions observed in Merapi lavas and contamination by pure limestone compositions accounts for a portion of the data (Fig. 8). These calculations are potentially only a minimum estimate of the importance of crustal material in the Merapi system, given the fact that the incorporation of solid crustal material, such as the xenoliths themselves, crystal transfer, and the buffering effect of mafic replenishment has not been taken into account in these models.

Contamination of magmas by upper crustal lithologies was largely discounted as a significant process at Merapi because of a lack of systematic variation between isotope ratios and SiO<sub>2</sub> (Gertisser & Keller, 2003; Debaille *et al.*, 2006). However, this argument assumes that the potential assimilant has considerably different SiO<sub>2</sub> (e.g. high SiO<sub>2</sub>) and given that carbonate and volcanoclastic deposits are the dominant lithologies beneath Merapi, sizeable amounts of assimilation may not have a significant effect on major element compositions, specifically SiO<sub>2</sub>. Using the most silica-rich contaminant modelled above, an addition of 10% crustal material would raise SiO<sub>2</sub> by only 3 wt%.

Thus, assimilation of crustal material at Merapi may be a significant process that is largely unaccounted for in current geochemical models. Of the magmatic phenocrysts analysed for Sr isotope zoning in this study, three out of four crystals appear to have xenocrystic cores and all have individual contaminated zones. An element of sampling bias may be a factor here, as large, complexly zoned

crystals were selected for drilling. However, a negative correlation between MgO wt%, FeO wt% and An mol% is observed in over 80% of the feldspar microprobe traverses (18 of 25 crystal traverses), and is clearly evident for feldspars with An mol%  $>85$  (Fig. 5), indicating that xenocrystic material is likely to be present in a significant percentage of Merapi crystals. Using a conservative estimate of 10–20% bulk xenocrystic material, a Merapi basaltic andesite with 60% crystals might contain between 6 and 12% crystalline material from non-magmatic crustal sources in addition to assimilated crustal melts that generate high <sup>87</sup>Sr/<sup>86</sup>Sr plagioclase overgrowth zones. Both anatectic melts and incorporated solids contribute to the range in Sr isotope ratios observed in the whole-rocks. This situation has significant implications for mass-balance calculations and geochemical modelling of the petrogenesis of Merapi magmas, as there is a significant late-stage crustal input that is not accounted for using the whole-rock data alone (e.g. Gertisser & Keller, 2003a; Debaille *et al.*, 2006).

Assimilation of carbonate sediment has the potential to alter the volatile budget of Merapi lavas significantly, which might influence the eruptive behaviour of the volcano. Conversion of limestone to a diopside–wollastonite assemblage, as seen in the Merapi calc-silicate xenoliths (Fig. 2), would liberate CO<sub>2</sub> (Goff *et al.*, 2001; Troll *et al.*, 2003; Gaeta *et al.*, 2006). This additional CO<sub>2</sub> would be relatively insoluble in the melt in a crustal basaltic andesite system (Holloway & Blank, 1994) and could result in rapid volatile saturation of the magma, potentially triggering an eruption. The abundance of calc-silicate xenoliths in the Merapi lavas indicates that the volatile budget of the Merapi magmas may have been significantly modified by carbonate assimilation prior to eruption.

## CONCLUSIONS AND IMPLICATIONS

Feldspar crystals present in recent Merapi basaltic andesite lavas exhibit measurable and significant Sr isotopic heterogeneity. Detailed investigation of these crystals and associated metasedimentary xenoliths indicates that there is a definite contribution from crustal rocks to the isotopic compositions and potentially the volatile budget of the Merapi magma system. Observed variations in <sup>87</sup>Sr/<sup>86</sup>Sr ratios within plagioclase crystals hosted in Merapi basaltic andesites appear to be the result of two main processes: (1) incorporation of xenocrysts sourced from a sedimentary protolith, forming high <sup>87</sup>Sr/<sup>86</sup>Sr, high An mol%, low MgO and low FeO plagioclase (Figs 5 and 6b–d); (2) crustal assimilation with combined fractional crystallization (AFC) forming magmatic rims and internal reaction zones (Fig. 6a) with generally increasing <sup>87</sup>Sr/<sup>86</sup>Sr and decreasing An mol% rim-ward. Unusually high anorthite

contents for feldspar in a basaltic andesite system and apparent decoupling of different chemical systems, such as An mol% and MgO and FeO (Fig. 5), can be resolved by the presence of non-magmatic crystal cores. A negative correlation between An mol% and MgO wt% has been noted in other settings (e.g. Kuritani, 1998); however, isotopic evidence is required for full identification of the source of this negative correlation. Our results imply that An mol% is not a reliable proxy for the degree of differentiation of the Merapi magma in which these crystals are found. This situation creates a need for improved models of geochemical mass-balance and temporal geochemical variations, which are currently based solely on whole-rock data for Merapi (Gertisser & Keller, 2003a; Debaille *et al.*, 2006). In addition, a significant contribution to the volatile budget of the Merapi magma via limestone assimilation could have profound effects on our understanding of the drivers for eruption at Merapi and other volcanoes sited on carbonate crust where calc-silicate xenoliths have been recognized, such as Popocatepetl, Mexico (Goff *et al.*, 2001), Pacaya, Guatemala (Janik *et al.*, 1992) and Vesuvius, Italy (Fulignati *et al.*, 2001). Our data indicate that shallow-level crustal contamination processes can be volumetrically significant although not clearly apparent using conventional geochemical techniques. This kind of assimilation can potentially influence the eruptive behaviour of explosive volcanoes, requiring a rethink of how such systems are evaluated by geochemists, petrologists and monitoring personnel.

## ACKNOWLEDGEMENTS

We are grateful to L. Schwarzkopf and M. Majhum for help during sample collection. We would like to acknowledge G. Nowell and T. Leeper for assistance with Sr isotope analyses, A. Calder for XRD analyses, and D. Rau for XRF analyses. Discussion with L. Schwarzkopf, J. Gamble, G. Wörner and D. Chertkoff, was much appreciated. Constructive and insightful reviews from V. Debaille, A. Renzulli, I. Smith and F. Tepley, and editorial comments from M. Wilson resulted in a significant improvement of the manuscript. We acknowledge financial support from the EC Marie Curie scheme, Enterprise Ireland, Science Foundation Ireland, and the Provost's Academic Development fund at Trinity College Dublin.

## REFERENCES

- Abratis, M., Schmincke, H.-U. & Hansteen, T. H. (2002). Composition and evolution of submarine volcanic rocks from the central and western Canary Islands. *International Journal of Earth Sciences* **91**, 562–582.
- Bahar, I. (1984). Contribution à la connaissance du volcanisme Indonésien: le Merapi (Centre Java); cadre structural, pétrologie, géochimie et implications volcanologiques. Ph.D. thesis, Université des Sciences et Techniques du Languedoc, Montpellier.
- Baker, C. K. & Black, P. M. (1980). Assimilation and metamorphism at a basalt-limestone contact, Tokatoka, New Zealand. *Mineral Mag.* **43**, 797–807.
- Balazs, D. (1968). *Karst Regions in Indonesia: Karszt-Es Barlangkutatas, Volume V*. Globus nyomda Budapest 61 pp.
- Barnes, C. G., Prestvik, T., Sundvoll, B. & Surratt, D. (2005). Pervasive assimilation of carbonate and silicate rocks in the Hortavaer igneous complex, north-central Norway. *Lithos* **80**, 179–199.
- Barton, M. D., Ilchik, R. P. & Marikos, M. A. (1991). Metasomatism. In: Kerrick, R. M. (ed.) *Contact Metamorphism. Mineralogical Society of America, Reviews in Mineralogy* **26**, 321–350.
- Beard, J. S. & Borgia, A. (1989). Temporal variation of mineralogy and petrology in cognate gabbroic enclaves at Arenal volcano, Costa Rica. *Contributions to Mineralogy and Petrology* **103**, 110–122.
- Beauducel, F. & Cornet, F. H. (1999). Collection and three-dimensional modeling of GPS and tilt data at Merapi volcano, Java. *Journal of Geophysical Research* **104**, 725–736.
- Bindeman, I. N., Ponomareva, V. V., Bailey, J. C. & Valley, J. W. (2004). Volcanic arc of Kamchatka: a province with high- $\delta^{18}\text{O}$  magma sources and large-scale  $^{18}\text{O}/^{16}\text{O}$  depletion of the upper crust. *Geochimica et Cosmochimica Acta* **68**, 841–865.
- Boudon, G., Camus, G., Gourgaud, A. & Lajoie, J. (1993). The 1984 nuée-ardente deposits of Merapi volcano Central Java, Indonesia: stratigraphy, textural characteristics, and transport mechanisms. *Bull. Volcanol.* **55**, 327–342.
- Bowen, N. L. (1940). Progressive metamorphism of siliceous limestones and dolomite. *Journal of Geology* **48**, 225–274.
- Camus, G., Gourgaud, A., Mossand-Berthommier, P.-C. & Vincent, P.-M. (2000). Merapi (Central Java, Indonesia): An outline of the structural and magmatological evolution, with a special emphasis to the major pyroclastic events. *Journal of Volcanology and Geothermal Research* **100**, 139–163.
- Charlier, B. L. A., Ginibre, C., Morgan, D., Nowell, G. M., Pearson, D. G., Davidson, J. P. & Ottley, C. J. (2006). Methods for the microsampling and high-precision analysis of strontium and rubidium isotopes at single crystal scale for petrological and geochronological applications. *Chemical Geology* **232**, 114–133.
- Clochiatti, R., Joron, J. L., Kerinec, F. & Treuil, M. (1982). Quelques données préliminaires sur la lave du dôme actuel du volcan Merapi (Java Indonésie) et sur ses enclaves. *Comptes Rendus de l'Académie des Sciences, Série A* **295**, 817–822.
- Curry, J. R., Shor, G. G., Raitt, R. W. & Henry, M. (1977). Seismic refraction and reflection studies of crustal structure of the eastern Sunda and western Banda arcs. *Journal of Geophysical Research* **82**, 2479–2489.
- Davidson, J. P. & Tepley, F. J., III (1997). Recharge in volcanic systems: Evidence from isotope profiles of phenocrysts. *Science* **275**, 826–829.
- Davidson, J. P., McMillan, N. J., Moorbath, S., Wörner, G., Russell, S. H. & Lopez-Escobar, L. (1990). The Nevados de Payachata volcanic region ( $18^{\circ}\text{S}/69^{\circ}\text{W}$ , N. Chile) II. Evidence for widespread crustal involvement in Andean magmatism. *Contributions to Mineralogy and Petrology* **105**, 412–432.
- Debaille, V., Doucelance, R., Weis, D. & Schiano, P. (2006). Multi-stage mixing in subduction zones: Application to Merapi volcano, (Java island, Sunda arc). *Geochimica et Cosmochimica Acta* **70**, 723–741.
- Deer, W., Howie, R. & Zussman, J. (1992). *An Introduction to the Rock-Forming Minerals*, 2nd edn. Harlow: Longman, 696 pp.
- de Genevraye, P. & Samuel, L. (1972). Geology of the Kendeng Zone (Central and East Java). *Proceedings, First Annual Convention, Indonesian Petroleum Association*, pp. 17–30.

- del Marmol, M. A. (1989). The petrology and geochemistry of Merapi Volcano, Central Java Indonesia. Ph.D. thesis, Johns Hopkins University, Baltimore, MD.
- Duncan, R. A. & Green, D. H. (1987). The genesis of refractory melts in the formation of oceanic crust. *Contributions to Mineralogy and Petrology* **96**, 326–342.
- Fulginiti, P., Kamenetsky, V. S., Marianelli, P., Sbrana, A. & Mernagh, T. P. (2001). Melt inclusion record of immiscibility between silicate, hydrosaline, and carbonate melts; applications to skarn genesis at Mount Vesuvius. *Geology* **29**, 1043–1046.
- Gaeta, M., Freda, C., Christensen, J. N., Dallai, L., Marra, F., Karner, D. B. & Scarlati, P. (2006). Time-dependent geochemistry of clinopyroxene from Alban Hills (Central Italy): Clues to source and evolution of ultrapotassic magmas. *Lithos* **86**, 330–346.
- Gasparon, M., Hilton, D. R. & Varne, R. (1994). Crustal contamination processes traced by helium isotopes: Examples from the Sunda arc, Indonesia. *Earth and Planetary Science Letters* **126**, 15–22.
- Gertisser, R. (2001). Gunung Merapi (Java, Indonesien): Eruptionsgeschichte und magmatische Evolution eines Hochrisiko-Vulkans. Ph.D. thesis, Albert-Ludwigs-Universität, Freiburg.
- Gertisser, R. & Keller, J. (2003a). Trace element and Sr, Nd, Pb and O isotope variations in medium-K and high-K volcanic rocks from Merapi Volcano, Central Java, Indonesia: Evidence for the involvement of subducted sediments in Sunda arc magma genesis. *Journal of Petrology* **44**, 457–489.
- Gertisser, R. & Keller, J. (2003b). Temporal variations in magma composition at Merapi Volcano (Central Java, Indonesia): magmatic cycles during the past 2000 years of explosive activity. *Journal of Volcanology and Geothermal Research* **123**, 1–23.
- Ginibre, C., Wörner, G. & Kronz, A. (2002). Minor- and trace-element zoning in plagioclase; implications for magma chamber processes at Parícuta Volcano, northern Chile. *Contributions to Mineralogy and Petrology* **143**, 200–315.
- Goff, F., Love, S. P., Warren, R. G., Counce, D., Obenholzer, J., Siebe, C. & Schmidt, S. C. (2001). Passive infrared remote sensing evidence for large, intermittent CO<sub>2</sub> emissions at Popocatepetl volcano, Mexico. *Chemical Geology* **177**, 133–156.
- Hamilton, W. (1979). *Tectonics of the Indonesian Region*. US Geological Survey, Professional Papers **1078**, 1–345.
- Hammer, J. E., Cashman, K. V. & Voight, B. (2000). Magmatic processes revealed by textural and compositional trends in Merapi dome lavas. *Journal of Volcanology and Geothermal Research* **100**, 165–192.
- Haryono, E. & Day, M. (2004). Landform differentiation within the Gunung Kidul Kegelkarst, Java, Indonesia. *Journal of Cave and Karst Studies* **66**, 62–69.
- Hemond, C. (1986). Géochimie isotopique du thorium et du strontium dans la série tholéiitique d'Islande et dans des séries calco-alcalines diverses. Thèse de III<sup>ème</sup> cycle, Université Paris VII, 151 pp.
- Hildreth, W. & Moorbath, S. (1988). Crustal contributions to arc magmatism in the Andes of Chile. *Contributions to Mineralogy and Petrology* **98**, 455–489.
- Holloway, J. R. & Blank, J. G. (1994). Application of experimental results to C–O–H species in natural melts. In: Carroll, M. R. & Holloway, J. R. (eds) *Volatiles in Magma*. Mineralogical Society of America, Reviews in Mineralogy **30**, 187–230.
- Housh, T. B. & Luhr, J. F. (1991). Plagioclase–melt equilibria in hydrous systems. *American Mineralogist* **76**, 477–492.
- Janič, C. J., Goff, F., Fahlquist, L., Adams, A., Roldán, M. A., Chiperá, S., Trujillo, P. & Counce, D. (1992). Hydrogeochemical exploration of geothermal prospects in the Tecuamburro volcano region, Guatemala. *Geothermics* **21**, 447–481.
- Jarrard, R. D. (1986). Relations among subduction parameters. *Reviews of Geophysics* **24**, 217–284.
- Joesten, R. (1977). Mineralogical and chemical evolution of contaminated igneous rocks at a gabbro–limestone contact, Christmas Mountains, Big Bend region, Texas. *Geological Society of America Bulletin* **88**, 1515–1529.
- Joesten, R., Hill, J. & Van-Horn, S. R. (1994). Limestone assimilation and clinopyroxenite production along the contacts of a 9 metre alkali olivine basalt dike, Killala Bay, Ireland. *Geol. Soc. Am. Abs.* **26**, 476–476.
- Kerinec, F. (1982). Le Merapi, volcan actif d'arc insulaire (Java): pétrographie et géochimie des matériaux solides, implications géotectoniques. Thèse de III<sup>ème</sup> cycle, Université de Paris Orsay, 92 pp.
- Koulakov, I., Bohm, M., Asch, G., Luehr, B.-G., Manzanares, A., Brotopuspito, K. S., Fauzi, N., Purbawinata, M. A., Puspito, N. T., Ratomopurbo, A., Kopp, H., Rabbel, W. & Shevkunova, E. (2007). P- and S-velocity structure of the crust and the upper mantle beneath Central Java from local tomography inversion. *Journal of Geophysical Research* (in press).
- Kuritani, T. (1998). Boundary layer crystallization in basaltic magma chamber: evidence from Rishiri volcano, northern Japan. *Journal of Petrology* **39**, 1619–1640.
- Lentz, D. R. (1999). Carbonatite genesis: a re-examination of the role of intrusion-related pneumatolytic skarn processes in limestone melting. *Geology* **27**, 335–338.
- Luais, B. (1986). Pétrologie et géochimie (éléments traces et rapports isotopiques du Sr) du magmatisme associé aux zones de subduction: exemples du bassin méditerranéen (Santorin, Arc Egéen; Stromboli, Arc Eolien) et des îles de la Sonde (Merapi, Java). Thèse de III<sup>ème</sup> cycle, Université des Sciences et Techniques du Languedoc, Montpellier, 255 pp.
- Milke, R. & Metz, P. (2002). Experimental investigation of the kinetics of the reaction wollastonite, calcite, anorthite, grossular, CO<sub>2</sub>. *American Journal of Science* **302**, 312–343.
- Owens, B. E. (2000). High-temperature contact metamorphism of calc-silicate xenoliths in the Kiglapait Intrusion, Labrador. *American Mineralogist* **85**, 1595–1605.
- Perini, G., Tepley, F. J., III, Davidson, J. P. & Conticelli, S. (2003). The origin of K-feldspar megacrysts hosted in alkaline potassic rocks from central Italy: a track for low-pressure processes in mafic magmas. *Lithos* **66**, 223–240.
- Ramos, F. C., Wolff, J. A. & Tollstrup, D. L. (2005). Sr isotope disequilibrium in Colombia River flood basalts: Evidence for rapid shallow level open system processes. *Geology* **33**, 457–460.
- Ratomopurbo, A. & Poupinet, G. (2000). An overview of the seismicity of Merapi volcano (Java, Indonesia), 1983–1994. *Journal of Volcanology and Geothermal Research* **100**, 193–214.
- Renzulli, A., Serri, G., Santi, P., Mattioli, M. & Holm, P. M. (2001). Origin of high-silica liquids at Stromboli volcano (Aeolian Islands, Italy) inferred from crustal xenoliths. *Bulletin of Volcanology* **62**, 400–419.
- Renzulli, A., Tribaudino, M., Salvioli-Mariani, E., Serri, G. & Holm, P. M. (2003). Cordierite–anorthoclase hornfels xenoliths in Stromboli lava (Aeolian Islands, Sicily): an example of a fast cooled contact aureole. *European Journal of Mineralogy* **15**, 665–679.
- Schwarzkopf, L. H., Schmincke, H.-U. & Troll, V. R. (2001). Pseudotachylite on impact marks of block surfaces in block-and-ash flows at Merapi volcano, Central Java, Indonesia. *International Journal of Earth Sciences* **90**, 769–775.
- Schwarzkopf, L. M., Schmincke, H.-U. & Cronin, S. J. (2005). A conceptual model for block-and-ash flow basal avalanche transport and deposition, based on deposit architecture of 1998 and 1994

- Merapi flows. *Journal of Volcanology and Geothermal Research* **139**, 117–134.
- Sisson, T. W. & Grove, T. L. (1993). Experimental investigations of the role of H<sub>2</sub>O in calc-alkaline differentiation and subduction zone magmatism. *Contributions to Mineralogy and Petrology* **113**, 143–166.
- Smyth, H. R., Hall, R., Hamilton, J. & Kinny, P. (2005). In: East Java: Cenozoic basins, volcanoes and ancient basement: *Proceedings, Indonesian Petroleum Association, Thirtieth Annual Convention & Exhibition*.
- Spera, F. J. & Bohron, W. A. (2001). Energy-constrained open-system magmatic processes I: General model and energy-constrained assimilation and fractional crystallization (EC-AFC) formulation. *Journal of Petrology* **42**, 999–1018.
- Surono, B. T., Sudarno, I. & Wiryojujono, S. (1992). *Map: Geology of the Surakarta–Girintoro Quadrangles, Java*. Scale 1:100 000, 2 sheets. Bandung: Geological Research and Development Centre.
- Thirlwall, M. F. (1991). Long-term reproducibility of multi-collector Sr and Nd isotope ratio analysis. *Chemical Geology* **94**, 85–104.
- Tilley, C. E. (1952). Some trends of basaltic magma in limestone syntaxis. *American Journal of Science* **250**, 529–545.
- Tracey, R. J. & Frost, B. R. (1991). Phase equilibria and thermobarometry of calcareous, ultramafic and mafic rocks, and iron formations. In: Kerrick, D. M. (ed.) *Contact Metamorphism. Mineralogical Society of America, Reviews in Mineralogy* **26**, 207–289.
- Tregoning, P., Brunner, F. K., Brock, Y., Puntodewo, S. S. O., McCaffrey, R., Genrich, J. F., Calais, E., Rais, J. & Subarya, C. (1994). First geodetic measurement of convergence across the Java Trench. *Geophysical Research Letters* **19**, 2135–2138.
- Troll, V. R. & Schmincke, H.-U. (2002). Magma mixing and crustal recycling recorded in ternary feldspar from compositionally zoned peralkaline ignimbrite 'A', Gran Canaria, Canary Islands. *Journal of Petrology* **43**, 243–270.
- Troll, V. R., Schwarzkopf, L. M., Gertisser, R., Buckley, C., Chadwick, J., Zimmer, M. & Sulistiyo, Y. (2003). Shallow-level processes and their impact on the eruptive behaviour in arc volcanoes: evidence from recent Merapi lavas. In: *Abstracts, State of the Arc Meeting, Portland, Oregon (2003)*.
- Turner, S. & Foden, J. (2001). U, Th and Ra disequilibria, Sr, Nd and Pb isotope and trace element variations in Sunda arc lavas: predominance of a subducted sediment component. *Contributions to Mineralogy and Petrology* **142**, 43–57.
- Untung, M. & Sato, Y. (1978). Gravity and geological studies in Java, Indonesia. *Geological Survey of Indonesia and Geological Survey of Japan, Special Publication* **6**, 207.
- Van Bemmelen, R. W. (1949). *The Geology of Indonesia. IA, General Geology*. The Hague: Government Printing Office.
- Voight, B., Constantine, E. K., Siswoidjono, S. & Torley, R. (2000). Historical eruptions of Merapi Volcano, Central Java, Indonesia, 1768–1998. *Journal of Volcanology and Geothermal Research* **100**, 69–138.
- Wagner, D., Koulakov, I., Rabbel, W., Luehr, B.-G., Wittwer, A., Kopp, H. & the MERAMEX Scientists (2007). Joint Inversion of active and passive seismic data in Central Java. *Geophysical Journal International* (in press).
- Waight, T. E., Baker, J. A. & Peate, D. W. (2002). Sr isotope ratio measurements by double focusing MC-ICPMS: techniques, observations and pitfalls. *International Journal of Mass Spectrometry* **221**, 229–244.
- Waltham, A. C., Smart, P. L., Friederich, H., Eavis, A. J. & Atkinson, T. C. (1983). The caves of Gunung Sewu, Java. *Cave Science* **10**, 55–96.
- Wenzel, T., Baumgartner, L. P., Brüggemann, G. E., Konnikov, E. G. & Kislov, E. V. (2001). Partial melting and assimilation of dolomitic xenoliths by mafic magma. *Terra Nova* **13**, 197–202.
- Wenzel, T., Baumgartner, L. P., Brüggemann, G. E., Konnikov, E. G., Kislov, E. V. & Orsoev, D. A. (2002). Partial melting and assimilation of dolomitic xenoliths by mafic magma: the Ioko-Dovyren intrusion (north Baikal region, Russia). *Journal of Petrology* **43**, 2049–2074.
- Westerhaus, M., Rebscher, D., Welle, W., Pfaff, A., Körner, A. & Nandaka, I. G. M. (1998). Deformation measurements at the flanks of Merapi volcano. *Deutsche Geophysikalische Gesellschaft, Mitteilungen, Sonderband III*, 3–8.
- Wilson, M. (1989). *Igneous Petrogenesis*. London: Chapman & Hall, 466 pp.
- Wolff, J. A., Ramos, F. C. & Davidson, J. P. (1999). Sr isotope disequilibrium during differentiation of the Bandelier Tuff: Constraints on the crystallization of a large rhyolitic magma chamber. *Geology* **27**, 495–498.